J Mater Sci (2007) 42:7592–7600
DOI 10.1007/s10853-006-1326-7

Impression creep of monolithic and composite lead free solders

Purushotham K. Muthur Srinath · Pranesh B. Aswath

Received: 12 July 2005 / Accepted: 28 November 2006 / Published online: 26 April 2007

Abstract Even though several EMS (Electronic manufacturing services) companies are currently producing ''lead free'' products, a general notion of apprehension still exists in the industry, primarily due to the lack of sufficient mechanical reliability data supporting the use of lead free alloys. The current study was an effort to generate an understanding of the mechanisms of creep deformation in monolithic and composite (Ag and Cu reinforced) Sn–3.5Ag and Sn–3.0Ag–0.5Cu lead free alloys in the high stress high temperature regime. Small volume solder samples were reflowed using a custom built computer controlled resistance furnace. Impression creep testing was employed to determine the activation energy and stress exponent. A careful analysis of the collected data revealed the underlying creep mechanisms and the following conclusions could be made. Both Sn–3.5Ag and Sn–3.0Ag–0.5Cu exhibited higher creep resistance as compared to the eutectic tin–lead solder under all tested conditions, with the ternary lead free alloy marginally outperforming the binary lead free alloy. Composite solders performed better as compared to monolithic solders. Furthermore, Cu reinforced solders demonstrated higher creep resistance as compared to Ag reinforced solders.

P. K. Muthur Srinath · P. B. Aswath (✉)
Materials Science and Engineering Program, University of Texas at Arlington, 500 West First Street, Arlington, TX 76019, USA
e-mail: aswath@uta.edu

Introduction

Lead free solders

Lead–tin alloys have been serving the electronics industry as the board level interconnect material since its inception and more recently in flip chip interconnect. However, the ill effects of lead as a toxic contaminant and its potential health and environmental hazards have been known for a long time. Several environmental regulations curbing the use of lead in electronics have been proposed by authorities worldwide. A large number of lead free alloys have been developed of which Sn–3.5Ag and Sn–3.0Ag–0.5Cu alloys have been widely accepted as replacement to the lead bearing solders.

The thermo-mechanical reliability of solders has gained significant attention in recent times due to the large gamut of applications especially in harsh environmental conditions that they are employed. Creep deformation in solders is considered as one of the prime failure mechanisms leading to premature failure in solder interconnects under such conditions [1–9]. Various avenues have been pursued in order to increase the creep resistance of solder interconnects, among them the composite solders approach has shown much promise [10–14]. This approach involves incorporating micro/nano sized metallic, intermetallic or ceramic particulates in the solder matrix. These particulate reinforcements hinder the movement of dislocations thereby increasing the resistance to deformation.

Impression creep

As the melting temperature of solders is quite low, room temperature is generally more than half the homologous temperature and the normal operating temperatures may

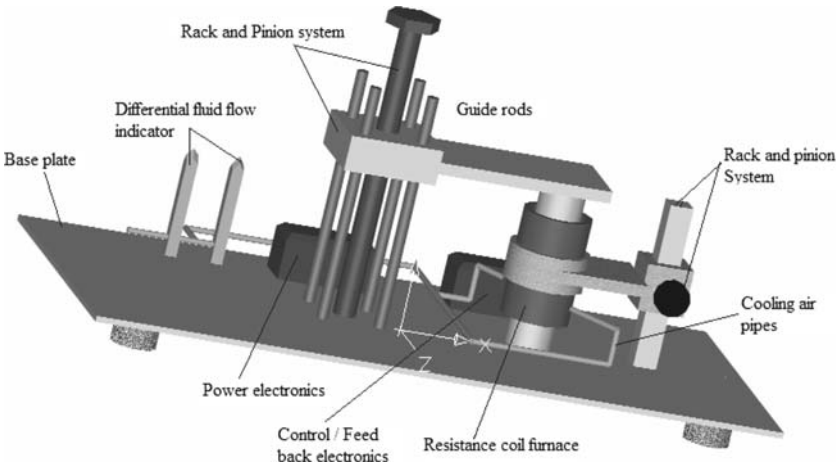

Fig. 1 AutoCAD drawing of the home built reflow soldering setup

reach as much as 0.8 times the homologous temperature. Under such circumstances, creep deformation is a predominant mode of failure in solder interconnects. With increasing functionality and performance, the current densities and consequently the thermal generation due to joule heating continue to increase. Failures due to creep deformation will continue to be an important mechanism that cannot be ignored in next generation devices having a large number of smaller sized I/O's operating under high current densities and employed in harsh environments.

Indentation testing of materials has been conducted for a long time in order to determine the static plastic properties of materials such as hardness, yield stress, etc. In the 70's, Yu and Li developed an indentation testing methodology to investigate creep properties in materials [15, 16]. In this technique, an indenter or a punch is forced into the sample surface by the application of a load and the depth of indentation is measured as a function of time. Various investigators have considered several indenter geometries in the past such as conical, pyramidal, spherical, cylindrical, etc. However, it has been noted that indentation creep tests using conical, pyramidal and spherical indenters do not show a steady state creep at constant load. A cylindrical punch or indenter with a flat end gives a steady state penetration velocity at constant load. This special type of indentation creep is referred to as impression creep [16].

As compared to a conventional uniaxial tensile creep test, the impression creep test has several advantages. First, impression creep tests require smaller samples and as a result homogeneous temperatures can be obtained throughout the material being tested unlike the conventional tensile creep where temperature homogeneity across the entire specimen volume is a highly debated topic. The second advantage of the impression creep technique is that a near constant stress can be obtained from constant loads as there is no effect of the cross sectional area as compared to the uniaxial tensile creep test which involves necking of the sample. As a result, the tertiary stage of the creep curve is absent in the impression creep response of a material. However, frictional or slack effects arising due to the contact of the indenter surface with the sample as the indentation depth increases restricts achieving a perfect load–stress conversion. Third, as compared to a conventional creep test, the impression creep test requires a significantly shorter time as the equivalent strain rate of impression creep is considerably higher than that of tensile creep under the same conditions. Lastly, and perhaps the most important advantage of impression creep are the small sample sizes and therefore the representative microstructures (similar to those found in actual reflowed solder interconnects) that can be tested.

Experimental details

Solder reflow apparatus

The reflow equipment (Fig. 1) was built with an intention to mimic the actual reflow process followed in electronic industries. It is a completely closed loop system consisting of a resistance coil furnace and a computer control. The computer control enables to obtain a reflow profile with temperature and time tolerances of ±5 °C and ±1 s, respectively.

Sample preparation

As the intention of this investigation was to follow the standard reflow process used in electronic assemblies, a sample preparation technique was devised which would deviate the least from such standard processes. Thus solder samples were reflowed on a copper substrate. About 3/8 inch (9.5 mm) diameter rods of oxygen free 101 copper were obtained from McMaster Carr. These rods were cut into discs of 2 mm thickness and polished and cleaned.

The solder pastes of Sn–37Pb, Sn–3.5Ag and Sn–3.0Ag–0.5Cu were obtained from Alpha Metals. For making samples of monolithic solders, the paste was used as shipped whereas for composite solders, a completely different processing route was followed. Spherical particulate reinforcement of 99.99% pure copper having a mean diameter of 5 μ was obtained from Atlantic Equipment Engineers and 99.99% pure silver spherical particulate reinforcements having a mean diameter of 3 μ was obtained from Alfa Asear. These reinforcements (5 wt.% in both cases) were mechanically mixed with the lead free solder pastes for about 45 min to ensure a uniform distribution of the particles in the solder matrix. The prepared composite solders were filled in medical grade syringes and were refrigerated as recommended by the paste manufacturer. It was observed from experience that a solder paste weight of 0.3 g would result in a sample thickness of around 2.5 mm upon reflow on a 3/8 inch (9.5 mm) diameter copper substrate. This thickness met the minimum necessary condition of sample thickness for indentation creep testing, which has been reported as five times the indenter diameter [17].

For each sample, 0.3 g of paste was directly dispensed from the syringe onto the fluxed copper substrate. A K type thermocouple was attached to the bottom of the copper substrate with adhesive backed Kaptone (Polyimide) disc of 3/8 inch diameter procured from McMaster Carr. The sample was then placed in the reflow chamber. Using the software interface, the ramp rates were set for each of the three reflow zones that included a reflow or dwell time of 30 s at 250 °C. After setting up the reflow parameters, the reflow was initiated. At the end of the reflow, the reflow chamber was retracted from the position so as to enable air cooling of the sample. Figure 2 shows the thermal profiles for a dwell time of 30 and 120 s obtained using the reflow setup. The reflowed sample so obtained was cleaned using acetone in an ultrasonic cleaner so as to remove the flux residue on the sample.

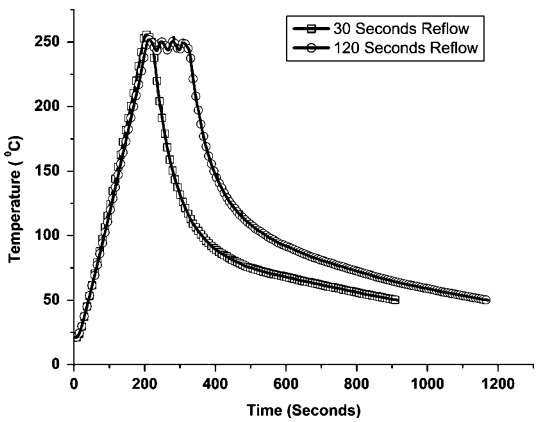

Fig. 2 Reflow profiles obtained using the home built system

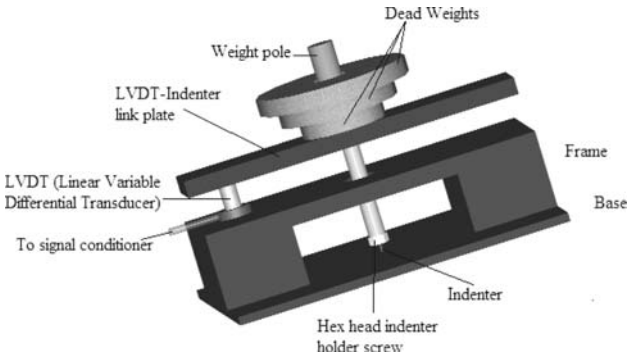

Fig. 3 AutoCAD drawing of Indentation Creep Test Setup

Impression creep test apparatus

The impression creep setup (Fig. 3) consists of a cylindrical indenter, a Linear variable differential transducer (LVDT), loading frame, data acquisition system and a thermal chamber. Various indenter sizes can be used on the system ranging from 50 to 500 μ. In the current investigation, a spring steel indenter having a diameter of 500 μ was used. The thermal chamber used was a Blue-M low temperature furnace having the capability to operate at temperatures of 25–200 °C with a tolerance of ±1 °C.

Creep test procedure

The entire impression creep setup was placed in a BlueM thermal chamber. At the beginning of each test, the position of the indenter was held in the unloaded state using a mechanical stop and the dead weights were placed. In the current study, each alloy system was tested under three different loads at 125 °C to determine the stress exponent. The construction of the equipment was such that the self-weights of mechanical linkages and components between the dead weight and the indenter also contributed to the total load. As a result, this load component was also taken into consideration in calculating the final applied stress. The three resultant stresses used in the current investigation were 30, 45 and 65 MPa. In the current investigation, each alloy system was tested at 75, 100 and 125 °C in order to determine the activation energy for creep. A thermocouple was placed in the vicinity of the test sample inside the thermal chamber in order to note the temperature stability during the test period. Upon achievement of a stable temperature, the mechanical stop was slowly retracted using a manually operated actuator so as to release the load on to the sample via the indenter. At the same time, the data collection was started using the desktop computer.

Generally each of the tests was run for a period of 3 h (some tests in which indentation depth was greater than 2,000 μ were run for a shorter time and the data was extrapolated for 3 h) and the temperature of the test chamber was noted during the entire test period to evaluate the temperature stability. At the end of the test, the thermal chamber was switched off and allowed to cool and subsequently the indenter was retracted back to the unloaded position and was restrained by the mechanical stop. The sample was removed from the sample stage and was stored for further microstructural analysis.

Results and discussion

In the current investigation, Sn–3.5Ag, Sn–3.0Ag–0.5Cu monolithic solders and their copper and silver reinforced composite counterparts were evaluated for creep. Impression creep tests were conducted at three different stress levels of 30, 45 and 67.5 MPa at 125 °C (Fig. 4a). From the creep data obtained, the steady state secondary creep strain rate was evaluated and this was used to obtain a plot of natural logarithm of stress versus natural logarithm of steady state creep rate (Fig. 5). The stress exponent was evaluated by determining the slope of this plot. In order to determine the activation energy, impression creep tests were conducted at temperatures of 75, 100 and 125 °C and a stress of 30 MPa. Form the above data (Fig. 4b), a plot of reciprocal of temperature in Kelvin versus the natural logarithm of the steady state creep rate was plotted (Fig. 6) to obtain the activation energy.

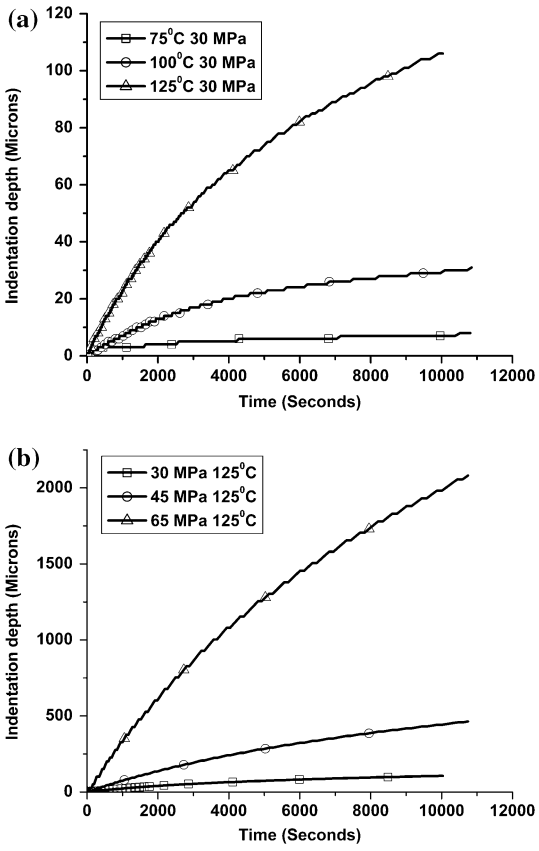

Fig. 4 Plots illustrating indentation creep data for Sn–Ag–Cu + 5% Cu, (**a**) activation energy creep data (varying test temperatures) and (**b**) Stress exponent creep data (varying punch stress)

Creep mechanisms in Sn–Pb eutectic solder and Sn–Ag and Sn–Ag–Cu lead (Pb) free solders, a comparison

It is quite evident that all the lead free systems perform much better than the lead–tin eutectic that has the lowest activation energy (Refer Tables 1 and 2) among all. The reason for this being that the microstructure of lead–tin coarsened after subjecting it to high temperature creep test due to its completely soluble nature. Another reason being that tin and lead do not form any intermetallics in the bulk of the solder as generally found in the lead free systems tested. Intermetallics in the bulk of the solder resist the motion of dislocation movement resulting in higher creep resistances.

It can be seen that the microstructure of eutectic Sn–Pb consists of a tin rich phase and a lead rich phase, since Sn-atoms and Pb-atoms have quasi equal shares in the Sn–Pb eutectic. Therefore, Sn-atoms and Pb-atoms need to change positions with each other before they can nucleate on their respective crystal. Thus, whichever phase grows faster depletes the region in front of its growth by the atoms of its own phase and will consequently be slowed down. Meanwhile the surrounding of the slower growing phase will be enriched by atoms of this phase, which accelerates its growth. In contrast, most of the Sn–Ag or Sn–Ag–Cu is

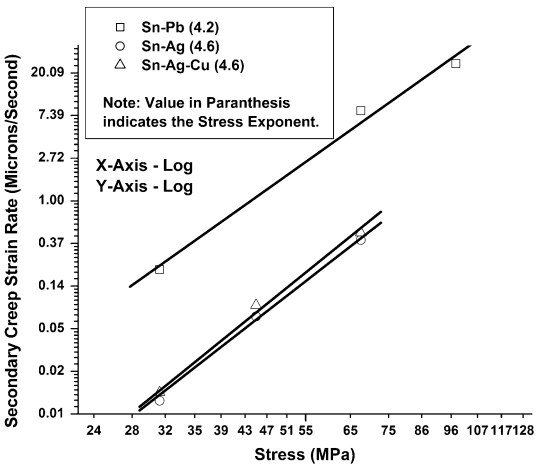

Fig. 5 Plot illustrating the difference in stress exponent between Pb bearing and Pb free solders

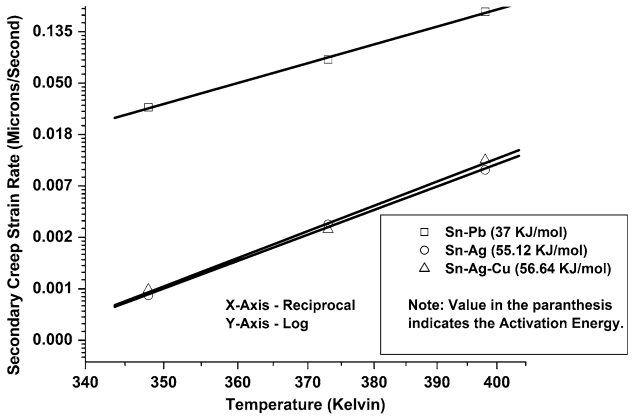

Fig. 6 Plot illustrating the difference in activation energy between lead (Pb) bearing and lead (Pb) free solders

comprised of Sn-atoms, so that the growing of tin crystals will not be significantly slowed down by depletion of the surrounding. The coupled growth in the Sn–Pb eutectic leads to a fine microstructure of equal sized grains of different phases. Therefore the Sn–Pb eutectic is able to deform superplastically (generally stress exponent n is close to 2).

Figures 7a–c and 8a–c represent the typical microstructures of eutectic Sn–Ag and the near eutectic Sn–Ag–Cu alloys processed under similar conditions of a 30-s reflow and air cooling. In contrast to eutectic Sn–Pb, the Sn–Ag and Sn–Ag–Cu microstructure is characterized by precipitates that are dispersed in the β-Sn-matrix, which leads to higher creep resistance due to the precipitation strengthening.

Values of 37 kJ/mol and 4.2 for the activation energy and the stress exponent, respectively, were obtained for the eutectic Sn–Pb alloy tested. The obtained activation energy is consistent with the value of 39.6 kJ/mol that corresponds to Sn diffusion in the Pb grain boundary [20]. Interface sliding may hence be considered as a possible creep mechanism in eutectic lead–tin at the tested temperature and stresses. The higher value of the stress exponent rules out the possibility of a superplastic behavior that is generally associated with lead–tin alloys. The reason for such behaviour can be explained by comparing the microstructures before (as reflowed) and after the test. Even though some amount of coarsening occurred during the high temperature creep, significant coarsening of the microstructure generally associated with long-term high temperature ageing was absent.

In contrast, the activation energy and stress exponent values of 55.12 kJ/mol and 4.6 for the eutectic Sn–Ag suggest that the dominant operating mechanism is dislocation climb. The creep response of Sn–3.5Ag alloy is primarily controlled by the divorced eutectic microconstituents that constitute the continuous matrix in which the β-Sn dendrites are embedded, since it is the slower creeping of the two constituents. The observed value of activation energy is very close to that of the activation energy for Ag diffusion in Sn i.e. 50 kJ/mol [21] (Table 2).

Table 2 Activation energies for various mechanisms in Sn-based solder systems

Mechanism	Activation energy (kJ/mol)
Sn diffusion in Pb grain boundary [20]	39.6
Ag diffusion in Sn [21]	50
Dislocation pipe diffusion in pure Sn [22, 23]	40–65
Dislocation core diffusion in Sn [24, 25]	66–80
Pb diffusion in Pb grain boundary [19]	65.6
Self-diffusion of pure Pb [26]	104

Table 1 Activation energy and stress exponent for creep deformation

Solder system	Activation energy (kJ/mol)	Stress exponent
Sn–3.5Ag (monolithic) [this work]	55.12	4.6
Sn–3.5Ag + 5% Cu (composite) [this work]	63.33	4.6
Sn–3.5Ag + 5% Ag (composite) [this work]	59.5	3.4
Sn–3.5Ag–0.5Cu (monolithic) [this work]	56.64	4.6
Sn–3.5Ag–0.5Cu + 5% Cu (composite) [this work]	70.59	3.8
Sn–3.5Ag–0.5Cu + 5% Ag (composite) [this work]	63.04	4.4
Sn–37Pb (monolithic) [this work]	37	4.2
Sn–3.5Ag (high stress regime) [18]	66	9
Sn–3.5Ag (low stress regime) [18]	43–46	3
Sn–Pb (low temperature/high temperature) [19]	55/55	1–3.5/2–6
Sn–3.5Ag and Sn–4.0Ag–0.5Cu [13]	50	–
Sn–3.5Ag reinforced with Cu/Ag/Ni particles [13]	53–61.2	–

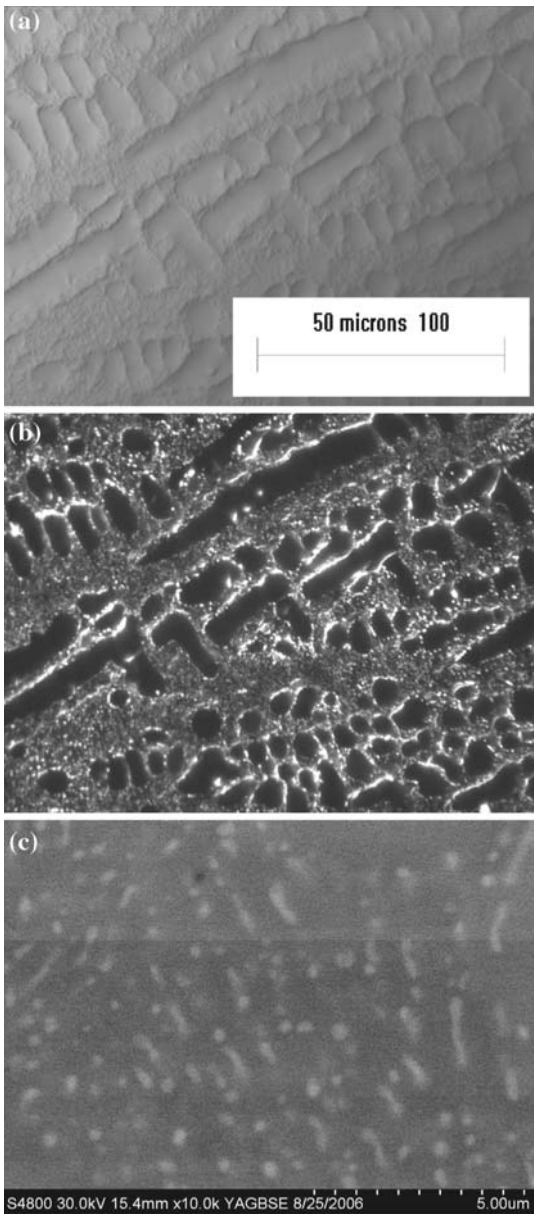

Fig. 7 (**a**) Polarized light image of Sn–Ag, (**b**) dark field optical image of Sn–Ag and (**c**) back scattered electron image of Sn–Ag. All samples reflowed at 250 °C for 30 s on a copper substrate and air cooled

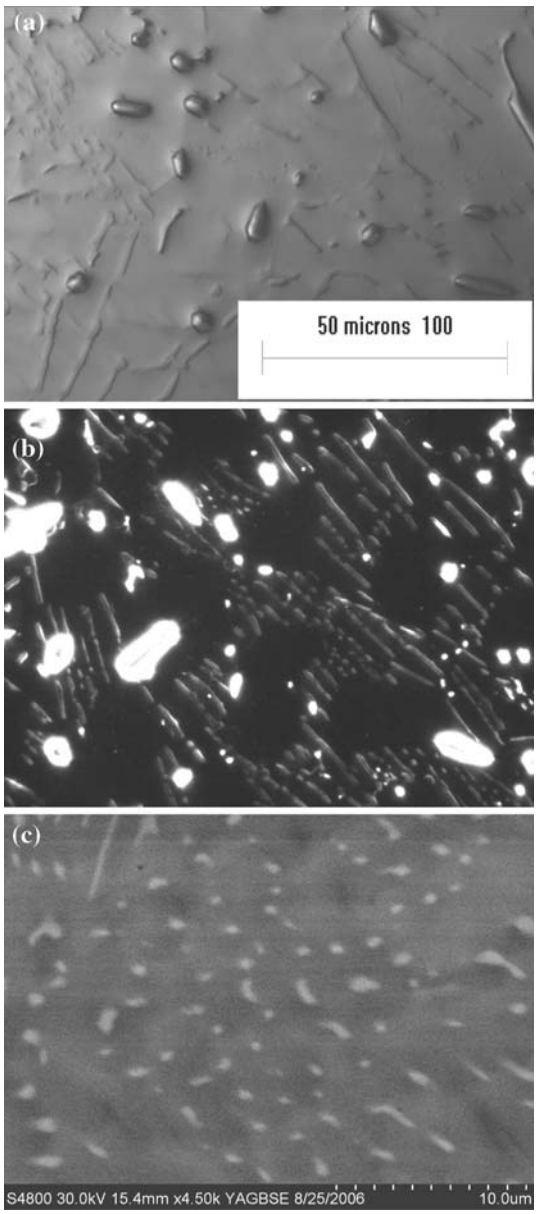

Fig. 8 (**a**) Polarized light image of Sn–Ag–Cu, (**b**) dark field optical image of Sn–Ag–Cu and (**c**) back scattered electron image of Sn–Ag–Cu. All samples reflowed at 250 °C for 30 s on a copper substrate and air cooled

The activation energy and stress exponent for Sn–3.0Ag–0.5Cu has been found to be 56.64 kJ/mol and 4.6. Comparing the microstructures of Sn–3.5Ag and Sn–3.0Ag–0.5Cu there is no significant difference between the two, except for small amount of Cu_6Sn_5 dispersed uniformly in the matrix of the ternary alloy. The values obtained for this alloy is very similar to those obtained for Sn–Ag as well and is in good agreement with the similar microstructures. It can hence be stated that the mechanism of creep in the binary and the ternary alloy under the conditions tested is dislocation climb controlled by diffusion of Ag in Sn.

Creep mechanisms in monolithic and composite lead (Pb) free solders, a comparison

It can also be seen that the composite lead free systems perform better in the temperature and stress range tested as compared to their monolithic counterparts (refer Figs. 9 and 10). One obvious reason being that the reinforcement particles provide a barrier for thermally activated dislocation motion that results in a higher creep resistance. The uniform distribution of Cu_6Sn_5 and Ag_3Sn intermetallics in the Cu and Ag reinforced Sn–3.5Ag solder can be seen in

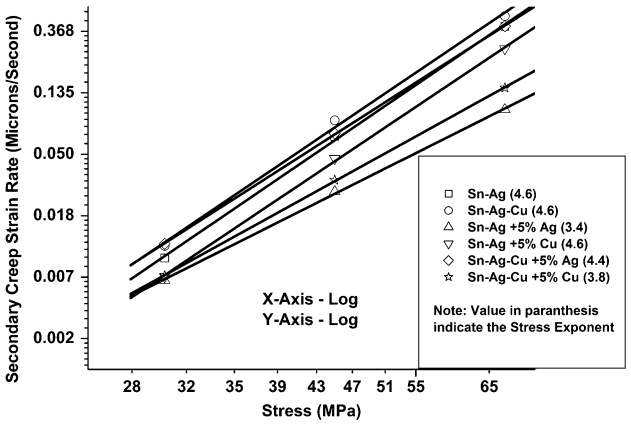

Fig. 9 Plot illustrating the difference in stress exponent between monolithic and composite lead (Pb) free solders

Fig. 11a, c, e and b, d, f, respectively. Another reason widely cited in literature is that the uniformly distributed reinforcement particles result in homogeneous deformation in the entire volume of the joint as compared to intense deformation at a local site [12].

As seen from the obtained data, Sn–3.5Ag + 5% Cu (composite) has creep activation energy of 63.33 kJ/mol and a stress exponent of 4.6. This is about 15% higher than the activation energy of its monolithic counterpart. These values of the creep parameters suggest that a dislocation climb controlled by dislocation pipe diffusion in pure tin (activation energy = 40–65 kJ/mol) is the dominant creep mechanism. Another interesting aspect is the difference between the Cu reinforced binary eutectic and the Ag reinforced binary eutectic. The Ag reinforced binary eutectic has activation energy of 59.5 and a stress exponent of 3.4. This difference in the activation energy has been thought to be due to the difference in the

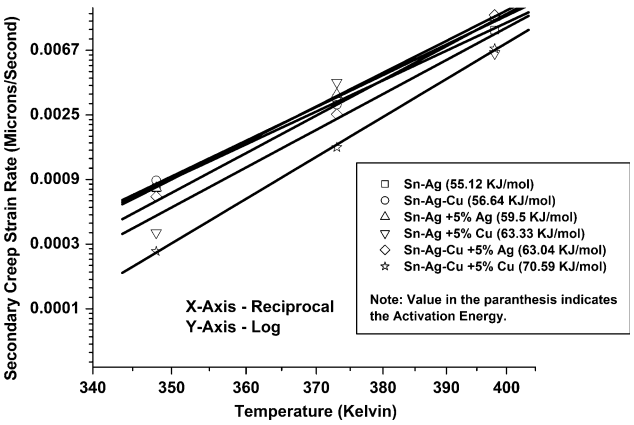

Fig. 10 Plot illustrating the difference in activation energy between monolithic and composite lead (Pb) free solders

diffusion of copper and silver in tin across their respective intermetallics. In the case of copper, there are two intermetallic layers, the metastable Cu_6Sn_5 and the thermodynamically stable Cu_3Sn that has known to be the diffusion rate limiting barrier for diffusion of Cu into Sn. However, the Ag diffusion into tin is not extremely curbed due to the presence of Ag_3Sn. It has also been reported that this difference in the activation energy between the Ag and Cu particle reinforced alloys may be attributed to the bonding strength of the two reinforcements to the primary matrix [27]. The Cu_6Sn_5 formed around the copper reinforcement during reflow has a weak interfacial bonding with the β-Sn matrix while the Ag_3Sn exhibits a stronger bonding with the β-Sn matrix. The weak interfacial bonding in copper reinforced alloys provides multiple nucleation sites for deformation throughout the entire solder joint this would promote homogenized deformation throughout the solder joint. Another reason that has been published in literature is their morphological difference, (refer to Fig. 11e and f), Cu_6Sn_5 is rod shaped requiring a higher climb height (energy) for dislocation motion while the Ag_3Sn is present as platelets which has a lesser climb height (energy) [28]. The dominant creep mechanism in Ag reinforced Sn–3.5Ag can be attributed to viscous glide limited by solute drag [18].

Similar to the behavior of the reinforced binary alloy, the particle reinforced ternary alloy also possesses better creep resistance than its monolithic counterpart due to reasons explained before. It was seen that the activation energy and stress exponent for the copper reinforced ternary were 70.39 kJ/mol and 3.8, respectively. This value is nominally consistent with the activation energy for dislocation core diffusion in tin, which has been reported as in the range of 66 kJ/mol [24] to 80 kJ/mol [25]. This combination of the alloy and reinforcement exhibits the best creep behavior among the materials tested. Thus a particle limited climb controlled by dislocation core diffusion can be stated as the predominant creep mechanism The creep activation energy and the stress exponent for the silver reinforced ternary alloy was found to be 63.04 kJ/mol and 4.4. These values relate to a particle limited climb controlled by dislocation pipe diffusion being dominant in both the systems. However, the higher activation energy of the copper reinforced Sn–3.0Ag–0.5Cu over that of its silver reinforced counterpart can be attributed to the difference in the diffusion kinetics of Cu and Ag into tin across their respective intermetallics. The ternary alloy and its composite counterparts show a higher creep resistance as compared to their binary counterparts, this may be attributed to the presence of additional Cu_6Sn_5 in the matrix of the ternary. The presence of copper also provides nucleation sites for the growth of Ag_3Sn in the ternary alloy.

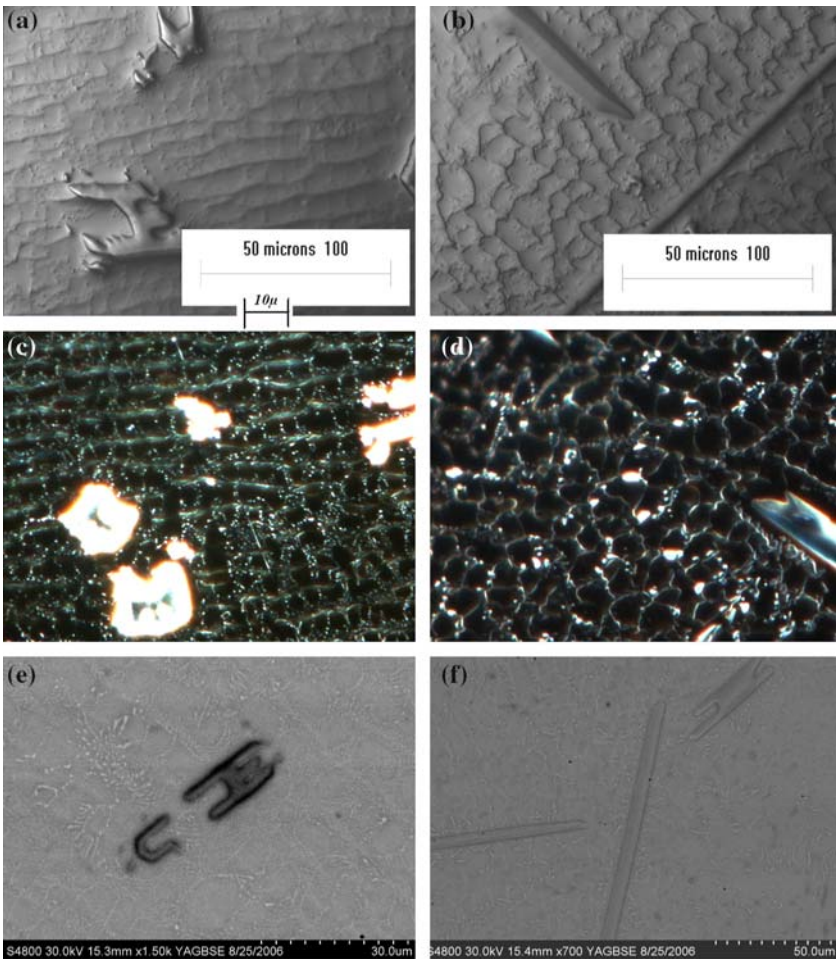

Fig. 11 Composite solder microstructures (**a**) polarized light image of Sn–Ag with 5% Cu reinforcement, (**b**) polarized light image of Sn–Ag with 5% Ag reinforcement, (**c**) dark field optical image of Sn–Ag with 5% Cu reinforcement, (**d**) dark field optical image of Sn–Ag with 5% Ag reinforcement, (**e**) backscattered electron image of Sn–Ag with 5% Cu reinforcement, (**f**) backscattered electron image Sn–Ag with 5% Ag reinforcement

Conclusion

Reflowed monolithic Sn–3.5Ag and Sn–3.0Ag–0.5Cu and their copper (Cu) and silver (Ag) reinforced composite counterparts were subjected to impression creep testing. The stress exponent and activation energy were determined in a high stress high temperature regime. It was found that all the lead free alloys exhibited better creep resistance as compared to lead–tin eutectic. Interfacial sliding was conceived to be the primary mechanism for creep deformation in the lead–tin eutectic alloy while in both the binary and ternary lead free alloys, dislocation climb was found to be the primary rate limiting mechanism. Composite solders performed better as compared to their monolithic alloys due to the formation of extensive intermetallics in the bulk. Particle limited dislocation climb was seen to be the primary operating mechanism in all the tested composite solders with the exception of Ag reinforced Sn–3.5Ag, in which particle limited glide was seen to be dominant. Copper acted as a superior reinforcement in limiting creep as compared to silver reinforcements. The monolithic ternary alloy also performed slightly better than the binary monolithic alloy.

Acknowledgements Support provided by Nokia USA and The Materials Science and Engineering Department at The University of Texas at Arlington is gratefully acknowledged.

References

1. Gibson AW, Choi S, Bieler TR, Subramanian KN (1997) In: Proceedings of the IEEE fifth international symposium on electronics and the environment, IEEE, Piscataway, NJ, p 246
2. Choi S, Subramanian KN, Bieler TR, Lucas JP (2000) J Electron Mater 29(10):1249
3. Frear DR (1991) Solder mechanics: a state of the art assessment. TMS, Warrendale, PA, p 191
4. Darveaux R, Murty KL, Turlik I (1992) J Miner Met Mater Soc 44:36
5. Murty KL, Turlik I (1992) In: Chen WT, Abe H (eds) Proceedings of the joint ASME/JSME advances in electronic packaging, vol EEP-1. ASME, New York, p 309
6. Morris JW Jr, Goldstein JLF, Mei Z (1993) J Miner Met Mater Soc 45:25
7. Morris JW Jr (1995) In: Shin KS et al (eds) Proceedings of the second Pacific Rim international conference on advanced materials

and processing. The Korean Institute of Metals and Materials, Seoul, Korea, p 715
8. Gibson AW, Choi S, Subramanian KN, Bieler TR (1997) In: Mahidhara RK et al (eds) Reliability of solders and solder joints. TMS, Warrendale, PA, p 97
9. Yang W, Messler RW, Felton LE (1994) J Electron Mater 23(8):765
10. Puttliz KJ, Stalter KA (2004) Handbook of lead free solder technology for microelectronic assemblies. Marcel Dekker
11. Guo F, Choi S, Lucas JP, Subramanian KN (2001) Solder Surf Mount Technol 13(1):7
12. Guo F, Choi S, Lucas JP, Subramanian KN, Bieler TR, Achari A, Paruchuri M (2003) Mater Sci Eng A351:190
13. Guo F, Lee J, Choi S, Lucas JP, Bieler TR, Subramanian KN (2001) J Electr Mater 30(9):1073
14. Choi S, Lucas JP, Subramanian KN, Bieler TR (2000) J Mater Sci: Mater Electr 11(6):497
15. Yang F, Li JCM (1995) Mech Mater 21:89
16. Li JCM (2001) Mater Sci Eng A 323:23
17. Chen H, Li JCM (1995) In: Chu SNG et al (eds) Micromechanics of advanced materials. TMS, Warrendale, PA, pp 367–371
18. Dutta I, Park C, Choi S (2004) Mater Sci Eng A 379:401
19. Yang F, Li JCM (1995) Mater Sci Eng A 201:40
20. Kim KK, Cupta D, Ho PH (1982) J Appl Phys 53:3620
21. Brandes EA, Brook GB (1992) Smithell's metals reference book, 7th edn. Butterworth-Heinemann
22. Darveaux R, Banerji K (1992) IEEE Trans Comp Hyb Manuf Technol 15:1013
23. Chu SNG, Li JCM (1979) Mater Sci Eng 39:1
24. Huang L, Wang L, Wu CML (2002) J Mater Res 17:2897
25. Song HG, Morris JW, Hua F (2002) Mater Trans 43:184
26. Lange W, Bergner D (1962) Phys Stat Soc 2:1410
27. Humphreys FJ, Kalu PN (1987) Acta Metall 35:2815
28. Guo F, Lee J, Subramanian KN (2003) Solder Surf Mount Technol 15(1):39